
Experimental and Numerical Study of Torsional Solid and Hollow Section of Polyolefin Fiber-Reinforced Concrete Beams

Iman H. Majeed^{1*}, Mazian A. Ahmad¹, Haleem K. Hussain¹
¹ Civil Engineering Department, Basrah University, Basrah, Iraq

*Corresponding author E-mail: pgs2350@uobasrah.edu.iq

(Received 9 Nov 2023, Revised 30 Nov 2023, Accepted 30 Nov 2023)

Abstract: An experimental and theoretical program was undertaken to enhance comprehension regarding how variations in fiber ratio impact the structural performance of both solid and hollow reinforced concrete beams when subjected to pure torsion. Polyolefin fiber was utilized in this study. To achieve this objective, a total of sixteen specimens of fiber-reinforced concrete beams were manufactured. Among these, eight were solid beams, while the remaining eight were hollow beams, all featuring rectangular cross-sections. These specimens were constructed employing polyolefin fiber. The findings indicated that incorporating polyolefin fiber into the concrete mixture led to improved mechanical properties in the cured concrete. The most significant enhancements were observed in the splitting tensile strength and flexural strength tests conducted on the specimens. Both solid and hollow beams exhibited notable enhancements in their torsional performance. These enhancements occurred as the polyolefin fiber percentage increased from zero to 1.5%, while the transverse and longitudinal reinforcement ratios remained constant. Furthermore, the reduction ratio of torsional strength becomes more noticeable when comparing solid and hollow sections in high-strength beams, as opposed to normal-strength beams.

Keywords: ultimate torsion, polyolefin fiber, solid beam, hollow beam, high strength, normal strength.

Introduction

Torsion can occur when external loads cause the beam to deviate significantly from its vertical bending plane, resulting in the twisting of the beam along its longitudinal axis. This twisting action, combined with bending moment and shear force. Torsion can be classified into two types: statistically determinate and statistically indeterminate. Figure 1 illustrates an example of a beam subjected to torsion. Torsion can occur through different means, such as reinforcing only one side of a slab or beam. Another way is by applying loads that cause significant rotation away from the diagonal axis to the longitudinal axis of the beam. In some cases, shear stresses can result in diagonal tensions, leading to the formation of diagonal cracks. Insufficient support for torsion can lead to sudden failure of the member [1].

Allawi [2] conducted that the strength of reinforced concrete (RC) beams under torsion was experimentally investigated using carbon fiber reinforced polymer (CFRP). The results of the study demonstrated that the ultimate torque increased by approximately 90% to 84%, depending on the specific strengthening pattern employed. When applying non-stop wrapping as a reinforcement technique, the cracking torque showed a substantial increase of 130% for hollow sections and 81% for solid sections in RC beams. These findings highlight the significant benefits of employing CFRP reinforcement for enhancing the torsional capacity of RC beams, particularly when utilizing non-stop wrapping. Al-Mahaidi [3], investigated the torsional strength of reinforced concrete (RC) beams with box and solid sections using both numerical and experimental approaches. The study focused on the application of carbon fiber reinforced polymer

(CFRP) laminates. The results of the study demonstrated a significant increase in both the ultimate strength and cracking strength of the beams. The ultimate strength saw an improvement of up to 78%, while the cracking strength increased by approximately 40%. These findings highlight the effectiveness of using CFRP laminates to enhance the torsional capacity of RC beams, offering substantial improvements in their overall structural performance. Mazin et.al [4], studied the Influence of fiber-type reinforcement on the torsional performance of solid and hollow reinforced concrete beams, an experimental approach was employed to investigate the impact of various fiber shapes and types on the behavior of solid and hollow reinforced concrete beams under torsion. Four fiber types, hooked end, straight, corrugated steel, and polyolefin were examined. Ten specimens were created, comprising five solid and five hollow beams with square cross-sections, each utilizing these different fibers. The findings revealed that the torsional behavior of both solid and hollow beams experienced notable improvement, particularly in cases where corrugated steel fiber was used for reinforcement. Although straight and polyolefin fibers slightly enhanced concrete properties and exhibited minor improvements in torsional capacity, beams reinforced with polyolefin fiber demonstrated enhanced ductility under torsion compared to the other fiber types.

This study involved the testing of 16 rectangular reinforced concrete beam specimens, which included both solid and hollow sections, under pure torsion. The investigation began by analyzing the mechanical properties of the concrete. The primary focus was then placed on studying the impact of beam types (hollow or solid sections) and various volume fractions of fibers on the torsional capacity of the beams. During the casting process, the beams were prepared with three different values of fiber volume fraction (VF): 0%, 0.5%, 1%, and 1.5%.

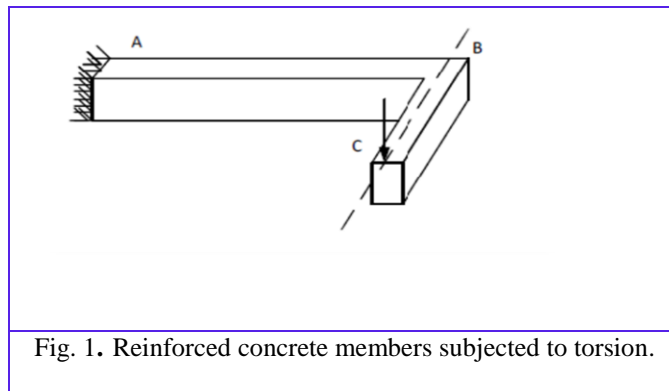


Fig. 1. Reinforced concrete members subjected to torsion.

1. Experimental Work

2.1. Material Properties

The physical and chemical properties of the cement used, as well as the mechanical properties of the fine and coarse aggregates, are presented in Tables 1 to 3, confirm with the ASTM standards [5-6]. Figure 2 shows the particle size distributions of the gravel (coarse aggregate) and sand (fine aggregate), obtained from local sources, Figure 3 shows the polyolefin fibers (PF) used in this study.

Table 4 provides details on the mechanical properties and geometric specifications of the polyolefin fiber used in the research. In this study, the concrete mix included PF at various ratios (0.5%, 1%, and 1.5%) by volume for all tested specimens. The chosen ratios were determined based on previous studies to ensure the desired workability and consistency of the fresh concrete [7-8].

Table 1 Physical properties of cement (ASTM C150-08)

Properties	Result	limits
Fineness (m^2/Kg)	305	≥ 280
Setting time (min.)		
Initial	132	≥ 45
Final	263	≤ 375
Compressive strength (N/mm^2)		
3 days	15.8	≥ 12
7 days	24.3	≥ 19

Table 2 Chemical composition of cement (ASTM C150-08)

Composition	Result Weight (%)	Limits (%)
Lime (CaO)	62.21	-
Silica (SiO ₂)	20.20	-
Alumina (Al ₂ O ₃)	5.13	-
Iron oxide (Fe ₂ O ₃)	3.21	-
Magnesia (MgO)	1.74	≤ 2.8
Sulfur trioxide (SO ₃)	2.92	≤ 5
Loss on Ignition	2.92	≤ 3

Table 3. Physical properties of aggregates (ASTM C33-18)

Property	Gravel	Sand
Bulk specific gravity	2.42	2.63
Apparent specific gravity	2.40	2.72
Dense dry density (kg/m ³)	1632	1870
Loose dry density (kg/m ³)	1452	1720
Sulphate content (%)	0.02	0.23
Absorption (%)	0.85	1.61



Fig. 2 Particle size distribution of fine and coarse aggregates.



Fig. 3. Polyolefin fiber.

Table 4. properties of polyolefin fiber

Shape	L(mm)	D (mm)	A.R.	f_t (MPa)
—	60	0.84	71	465

To conduct the testing, two types of concrete mixes were prepared: normal (NC) and high strength concrete (HC). PF was added to both mixes at three different ratios. The mix proportion of the control concrete mix utilized in the experiment is presented in Table 5. Sika visco-crete (5930) was used as a superplasticizer, with a ratio of approximately 1% of the total weight of cement. To assess the mechanical properties of the different concrete mixes, such as compressive strength, splitting tensile strength, and flexural.

Table 5. Proportion of control concrete mix

Parameter	Material quantity (25MPa)	Material quantity (55MPa)
Water/Cement ratio	0.48	0.30
Water (kg/m ³)	172	150
Cement (kg/m ³)	358	460
Sand (kg/m ³)	782	657
Gravel (kg/m ³)	1081	1138
Sika Visco Crete (kg/m ³)	3.4	4.6

2.2. Tested Beam Specimens

A comprehensive testing was conducted on a total of 16 reinforced concrete beams, focusing on pure torsion conditions. Table 6 outlines the distribution, indicating that eight beams were designed with a hollow cross section, while the remaining beams had solid cross sections. To facilitate comparison, a single reference beam specimen was prepared for each cross-sectional type, excluding any fiber-reinforced concrete. All beams shared identical dimensions, measuring 1400 mm in effected length, 150 mm in overall width, and 300 mm in overall depth. For the hollow beams, a specific wall thickness of 60 mm was implemented. Figure 4 visually presents the beam specimens, showcasing their geometry and reinforcement details.

Table 6. Details of tested beam specimens.

Normal Strength Specimens	High Strength Specimens	PFR %	Beam Sec.	Reinforcement	
				Long.	Stirrup
NS 00	HS 00	0.0	Solid		
NH 00	HH 00	0.0	Hollow		
NS 0.5	HS 0.5	0.5	Solid		
NH 0.5	HH 0.5	0.5	Hollow		
NS 1.0	HS 1.0	1.0	Solid		
NH 1.0	HH 1.0	1.0	Hollow		
NS 1.5	HS 1.5	1.5	Solid		
NH 1.5	HH 1.5	1.5	Hollow		

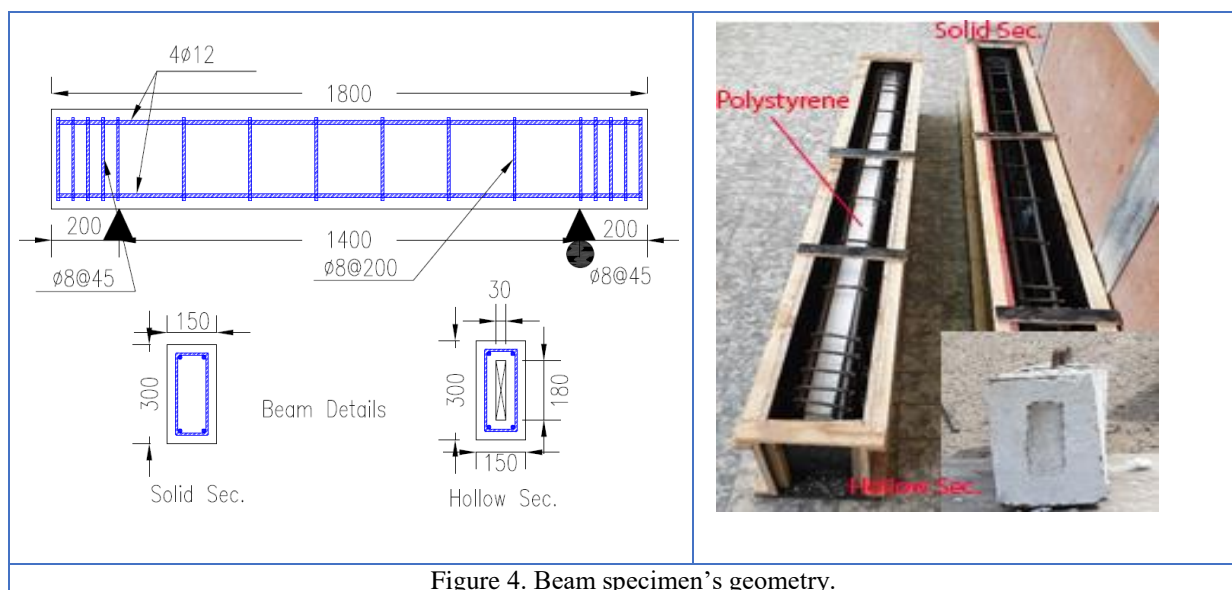


Figure 4. Beam specimen's geometry.

2.3. Test Procedure

The beam specimens underwent testing using a universal testing machine with a maximum capacity of 500 kN. Each beam was supported by two roller supports, and the load was transmitted through a load-spreader beam, which was an I-section steel girder. The support arms were securely fastened together with bolts and welded to the end roller supports, allowing the beam specimens to twist and elongate/shorten freely, as shown in Figure 5. To measure the twist angle, two LVDTs (linear variable differential transformers) were attached to the steel arm. A progressive increase in torque was applied in a continuous manner until the beams failed. Throughout the testing process, the applied torque and the corresponding angle of twist were recorded for each increment of load. The cracking torque, ultimate torque, and their respective angle of twist values were also documented.

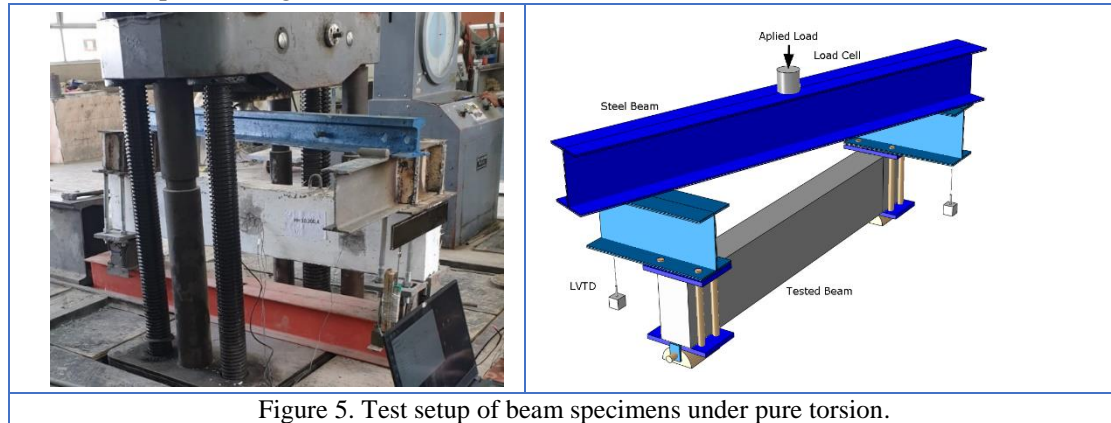


Figure 5. Test setup of beam specimens under pure torsion.

3. Finite Element Modeling

In this study, nonlinear finite element analysis was employed to model reinforced concrete beams using ABAQUS software (2022). The concrete, steel supports, steel plates (which surround the beam ends), and steel bolts (connecting the top and bottom of the plates) were defined as 3D solid stress element types. The steel reinforcement, both longitudinal and transverse, was defined as a 3D truss element type. The steel beams (I-section), used to apply the load, were defined as a 3D shell element type.

The loading and boundary conditions were applied in a manner similar to the experimental work. The ends of the beams were connected by clamped steel plates fastened with bolts, and the bottom plate was connected to steel supports with a free surface sliding capability to allow for twisting according to the applied load. The load was applied to the center of the top steel beam as a displacement, which transferred the displacement to the steel beams at the ends of the beam, resulting in twisting loads at the ends of the beam. The assembly of parts and boundary conditions is depicted in Figure 5.

3.1. Modeling Description

For the concrete, steel supports, plates, and bolt elements, we utilized 8-node hexahedral elements (C3D8R) with a mesh size of 25 mm. Additionally, employed 2-node elements (T3D2) to model the reinforcement bars, using the same 25 mm mesh size as that of the concrete elements. The steel beams were represented by 4-node elements (S4R) with the same mesh size.

The bond between the steel bars and concrete was simulated as an embedded perfect bond, while the interaction between the support and bottom end plate surfaces was defined as frictionless with hard contact. In contrast, the interaction between the concrete surface and the surrounding plates was defined as a friction penalty with hard contact. The mesh configuration of these elements can be observed in Figure 6.

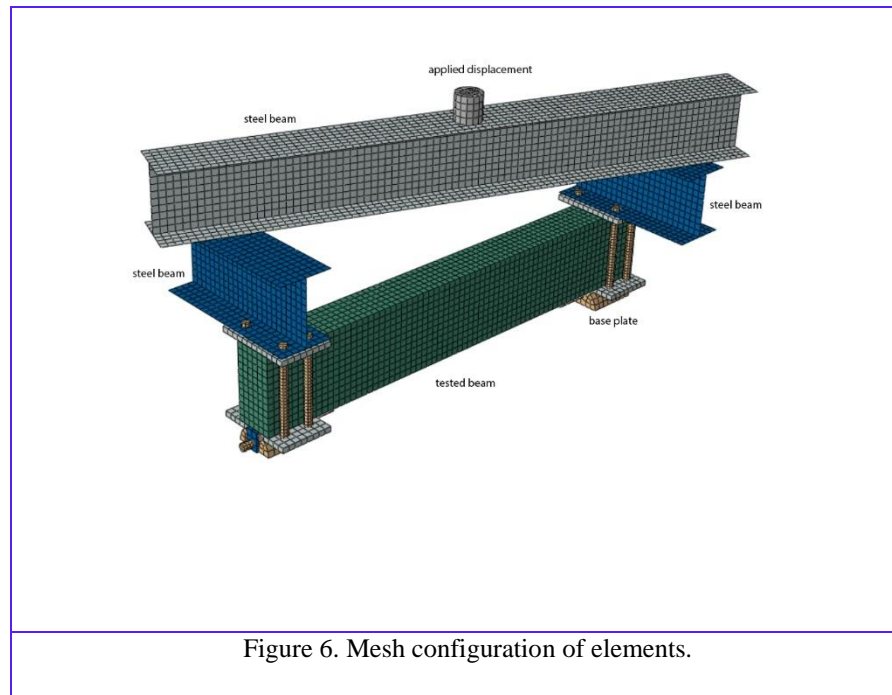


Figure 6. Mesh configuration of elements.

3.2. Material Modeling

3.2.1 Concrete Material

Concrete damage plasticity (CDP) model was used to modeling concrete material to consider the failure mechanisms of the concrete material for tensile cracking and compressive crushing. The Lubliner et al. introduced CDP [9] and Lee and Fenves developed it [10]. In this study, by using formal of BS EN 1992-1-1 2004 [11] to introduce the compression behavior of concrete which suitable for normal and high strength concrete and expressed as:

$$\sigma_c = f_c \frac{kn - n^2}{1 + (k - 2)n} \quad (1)$$

$$n = \frac{\varepsilon_c}{\varepsilon_{co}} \quad (2)$$

$$\varepsilon_{co} = 0.0007 \times f_c^{0.31} < 0.0028 \quad (3)$$

$$k = 1.05 \times E_c \times \frac{|\varepsilon_{co}|}{f_c} \quad (4)$$

$$E_c = 22 \times 10^3 (0.1f_c)^{0.3} \quad (5)$$

where, f_c is the concrete cylinder compressive strength; ε_c is the concrete compressive strain at any point, ε_{co} is the strain at peak stress, σ_c is the compressive stress of concrete and E_c is the young's modulus of concrete.

The compressive damage parameter can be represented by Eq.(6) [12].

$$dc = 1 - \frac{\sigma_c}{f'_c} \quad (6)$$

where, dc is the compression damage parameter.

The tensile stress–strain curve of concrete can be represented by Eq. (7) and Eq. (8) according to [13,14].

$$\sigma_t = E_c \varepsilon_t \quad \varepsilon_t \leq \varepsilon_{cr} \quad (7)$$

$$\sigma_t = f_{cr} \left(\frac{\varepsilon_{cr}}{\varepsilon_t} \right)^{0.4} \quad \varepsilon_t > \varepsilon_{cr} \quad (8)$$

The tensile damage parameter can be represented by Eq.(9) [15].

$$dt = 1 - \frac{\sigma_t}{f_t} \quad (9)$$

where, dt is the tension damage parameter.

Table 7 presents the experimental dataset used for modeling concrete material, providing insights into how PFR affects the specimens as shown in Figures 7 and 8 for stress-strain curves and Figures 9 and 10 for tensile stress-displacement curves, for NC and HC respectively.

Table 7. Data used for modeling concrete with PFR

Concrete Strength	PFR %	f_c MPa	f_t MPa	F_{cr} MPa	E_c MPa
Normal	0.0	26.3	3.45	4.13	24830
	0.5	25.1	4.11	6.15	21160
	1.0	26.8	5.82	6.41	19370
	1.5	25.3	6.15	7.78	17640
	0.0	56.3	6.30	6.88	38545
High	0.5	57.1	6.91	9.34	35360
	1.0	56.9	8.53	10.51	32175
	1.5	55.8	8.92	11.34	30720

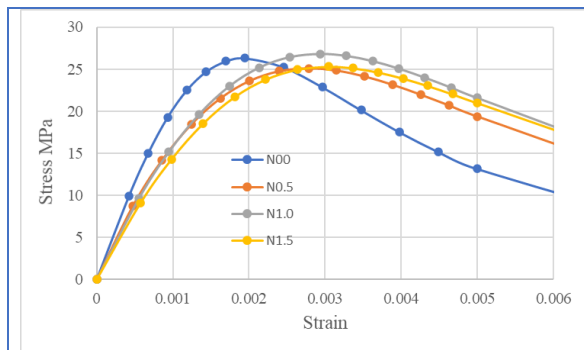


Figure 7. Stress-strain curves for NC with PFR

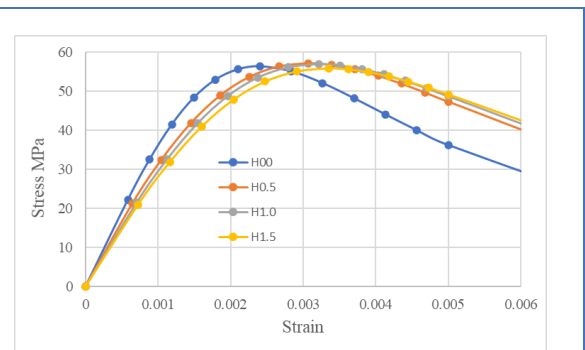


Figure 8. stress-strain curves for HC with PFR

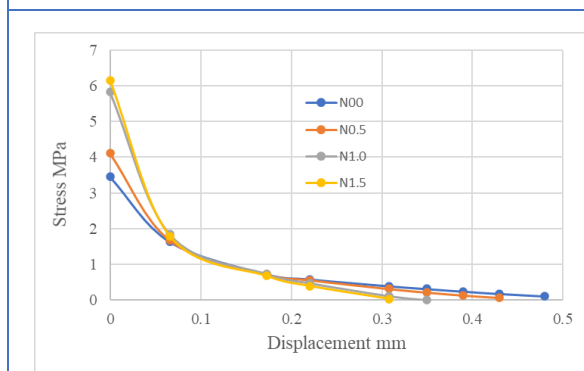


Figure 9. f_t stress-displacement curves for NC with PFR.

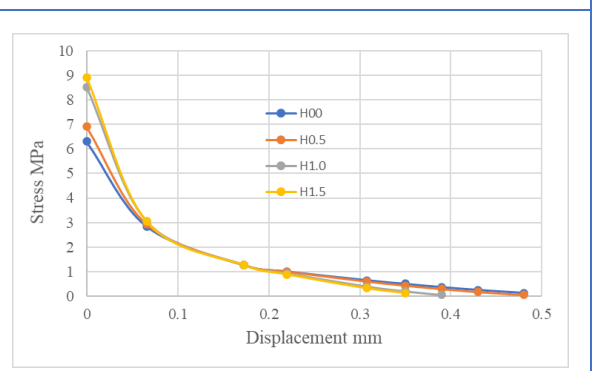


Figure 10. f_t stress-displacement curves for HC with PFR.

Table 8 displays the values of various parameters employed in the CDP model, derived from a synthesis of findings from multiple research studies [16,17].

Table 8 CDP parameters.				
ψ	e	fbo/fco	K	V
35	0.1	1.16	0.667	0

where, ψ = Dilation angle, e= Eccentricity, fbo/fco= Proportion between biaxial and uniaxial compressive strength, K= Shape parameter, and V= Viscosity Parameter.

3.2.2. Steel Reinforcement Material

The reinforcement was defined depend on the experimental results of the tensile tests. The behavior of stress -strain curve was defined according to British Standards Institution [11] by Eq.[10] and Eq.[11].

$$\sigma_s = \sigma_n(1 + \varepsilon_n) \quad (10)$$

$$\varepsilon_s^{pl} = \varepsilon_s - \varepsilon_s^{el} \quad (11)$$

where, $\varepsilon_s = \ln(1 + \varepsilon_n)$, $\varepsilon_s^{el} = \sigma_s / E_s$, σ_n is the nominal stress, ε_n is the nominal strain, and E_s is the steel modulus of elasticity (200 GPa).

3.2.3. Steel Plate, Bolt and Support Materials

These steel materials were defined as elastic behavior because it used for applying load and support specimens. The elastic behavior can be represented in program by Poisson ratio value ($\nu = 0.3$) and steel modulus of elasticity ($E_s = 200$ GPa).

4. Results and Discussion

4.1. Properties of Hardened Concrete

As illustrated in Table 7, adding PF to concrete does not have a significant impact on compressive strength. Meanwhile, the tensile strength exhibits a proportional increase with the addition of PFR. This effect is observed consistently for both NC and HC.

4.2. Experimental Results

The study found that employing a hollow cross-section has an impact on the torsional strength of reinforced concrete specimens as shown in Tables 9 and 10 . At the first crack, the torque load T_{cr} increased with increased PFR when the twist angle θ_{cr} showed a notable increase with 1.0% and 1.5% of PFR for both t_{type} sections and both concrete strengths. Also, The ultimate torque T_u and twist angle θ_u increase with an increase in PFR. This behavior may be due to the addition of PF, which increases the torsional stiffness of the reinforced concrete beam, leading to an increase in the maximum resisting torque. The study also found that the addition of PF increases the energy absorption capacity of the RC beam, leading to an increase in the maximum angle of twist as shown in Figures 11 to 14. Additionally, PF helps to delay the onset of cracking and improve the ductility of the RC beam.

Table 9. Torque and twist angle at first crack.

Spe.	Solid Sec.		Hollow Sec.	
	T_{cr}	θ_{cr}	T_{cr}	θ_{cr}
	kN.m	rad.	kN.m	rad.
N0.0	4.46	0.0025	3.23	0.0016
N0.5	5.04	0.0025	4.20	0.0011
N1.0	5.97	0.0045	5.75	0.0043
N1.5	6.82	0.0059	5.72	0.0047
H0.0	7.87	0.0012	6.57	0.0009
H0.5	8.17	0.0012	6.71	0.0005
H1.0	8.48	0.0018	7.65	0.0011
H1.5	10.08	0.0025	9.13	0.0023

Table 10. Torque and twist angle at ultimate torque

Spe.	Solid Sec.		Hollow Sec.	
	T_u	θ_u	T_u	θ_u
	kN.m	rad.	kN.m	rad.
N0.0	6.97	0.0400	5.33	0.0450
N0.5	9.19	0.0580	8.22	0.0440
N1.0	11.03	0.0740	10.06	0.0730
N1.5	12.15	0.0849	11.51	0.0839
H0.0	10.66	0.0087	9.36	0.0144
H0.5	12.07	0.0157	9.88	0.0142
H1.0	15.03	0.0370	12.38	0.0312
H1.5	15.53	0.0340	12.87	0.0331

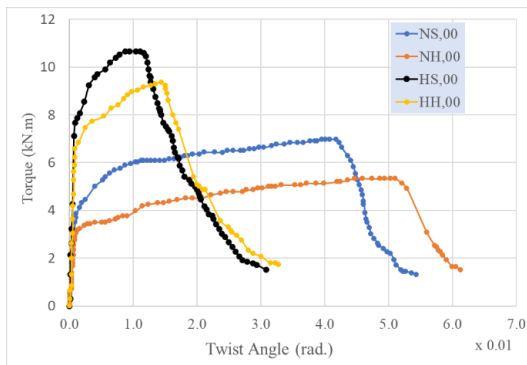


Figure 11 Torque-twist curve for PFR 0%

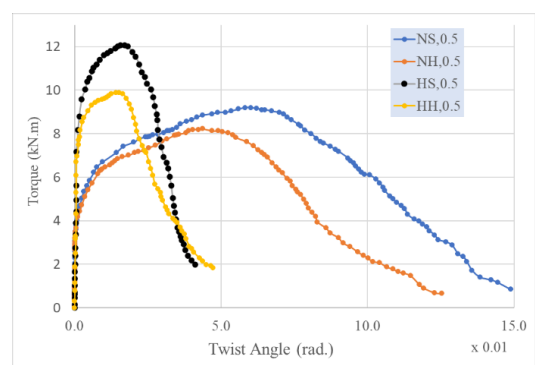


Figure 12 Torque-twist curve for PFR 0.5%

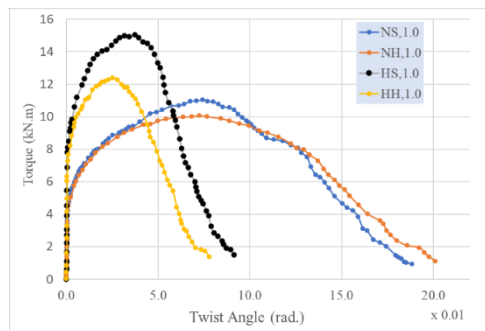


Figure 13 Torque-twist curve for PFR 1.0%

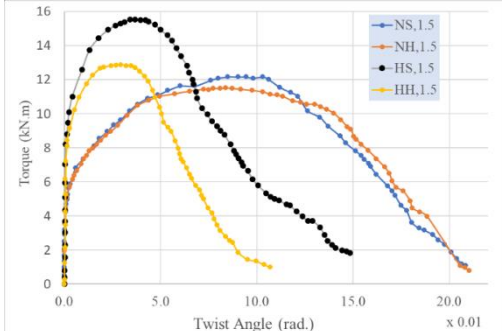


Figure 14 Torque-twist curve for PFR 1.5%

4.3. FEM Results

Table 11 shows the comparison between experimental and theoretical results for ultimate torsional loads. Figures 15 to 22 show the comparison between experimental and FEA for solid and hollow sections for PFR of reinforced concrete specimens of normal and high compressive strengths. The results and FEA specimens' behavior showed good agreement with experimental results for the selected model.

Table 11 Experimental and theoretical comparison

Spe.	EXP.		FEM		FEA/EXP	
	T_u	θ_u	T_u	θ_u	T_u	θ_u
	kN.m	rad.	kN.m	rad.		
NS00	6.97	0.04	6.80	0.043	0.98	1.08
NH00	5.33	0.045	5.53	0.052	1.04	1.16
NS0.5	9.19	0.058	9.51	0.057	1.03	0.98
NH0.5	8.22	0.044	7.96	0.052	0.97	1.18
NS1.0	11.03	0.074	10.17	0.078	0.92	1.05
NH1.0	10.06	0.073	9.23	0.088	0.92	1.21
NS1.5	12.15	0.085	12.60	0.085	1.04	1.00
NH1.5	11.51	0.084	10.42	0.087	0.91	1.04
HS00	10.66	0.009	10.05	0.01	0.94	1.15
HH00	9.36	0.014	9.81	0.013	1.05	0.90
HS0.5	12.07	0.016	11.27	0.018	0.93	1.15
HH0.5	9.88	$\frac{0.014}{2}$	10.04	0.013	1.02	0.92
HS1.0	15.03	0.037	13.87	0.026	0.92	0.70
HH1.0	12.38	0.025	11.38	0.021	0.92	0.84
HS1.5	15.53	0.034	14.32	0.04	0.92	1.18
HH1.5	12.87	0.029	11.83	0.032	0.92	1.10

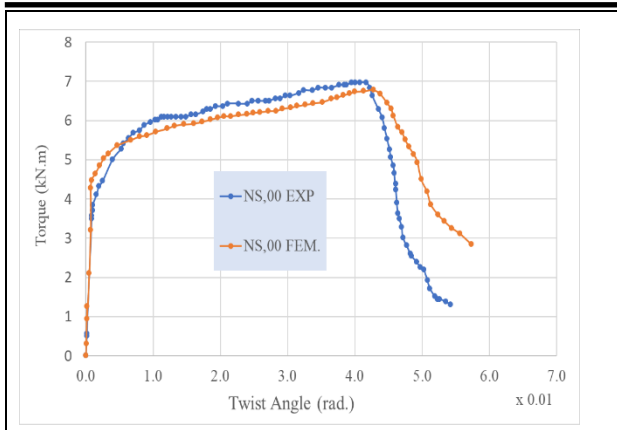


Figure 15 Torque-twist curve for PFR 0.0% (NC- Solid Sec.)

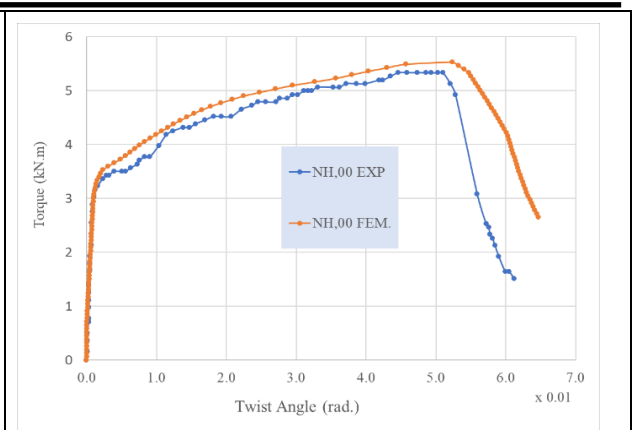


Figure 16 Torque-twist curve for PFR 0.0% (NC-Hollow Sec.)

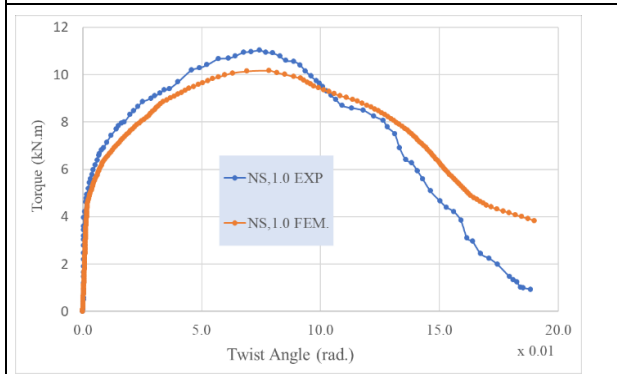


Figure 17 Torque-twist curve for PFR 1.0% (NC- Solid Sec.)

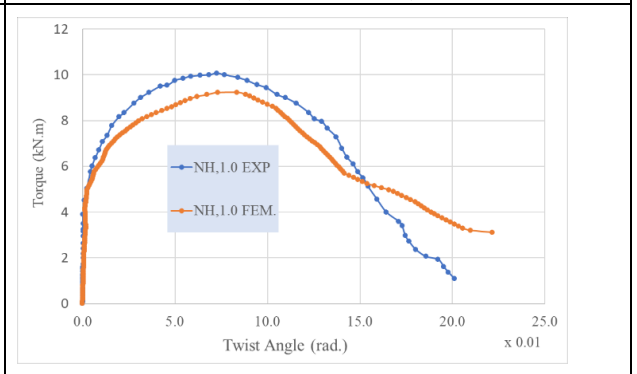


Figure 18 Torque-twist curve for PFR 0.0% (NC-Hollow Sec.)

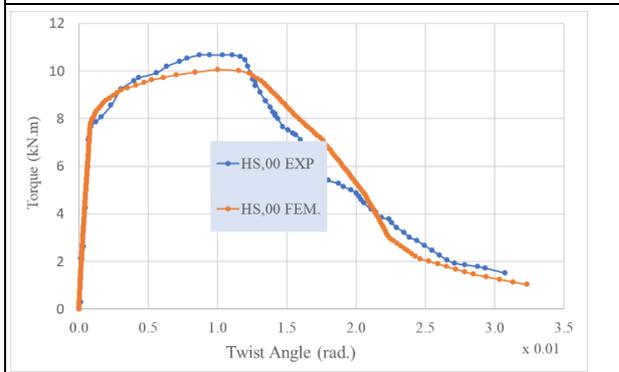


Figure 19 Torque-twist curve for PFR 0.0% (HC- Solid Sec.)

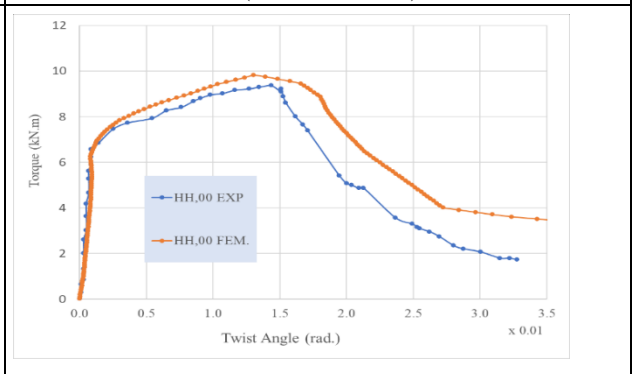


Figure 20 Torque-twist curve for PFR 0.0% (HC-Hollow Sec.)

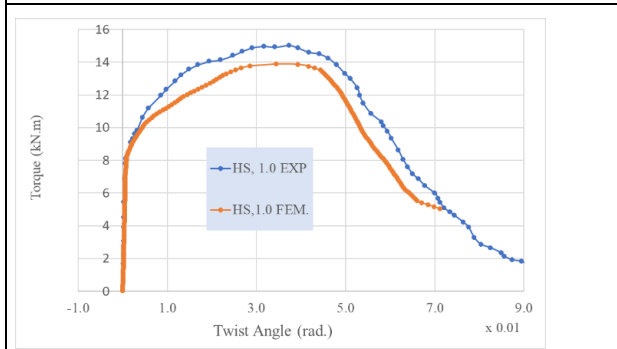


Figure 21 Torque-twist curve for PFR 1.0% (HC- Solid Sec.)

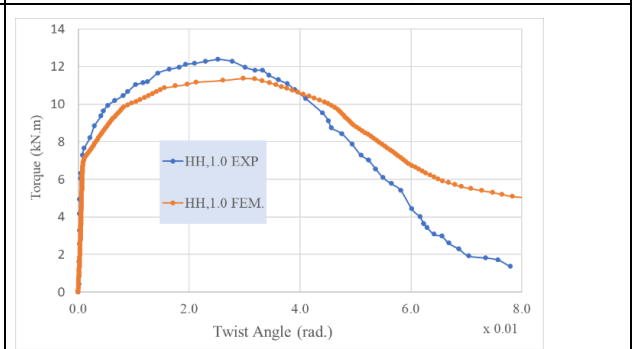


Figure 22 Torque-twist curve for PFR 1.0% (HC-Hollow Sec.)

4.4 Failure Mods

Figure 23 illustrates the observed failure modes during the experimental testing of the specimens subjected to torsional loads. When these members were subjected to torsion, the shearing stresses, resulting in inclined ring-shaped stress patterns. It is clearly observe that the reference beams with 0.0% PFR for both strength levels of concrete, normal and high, exhibited failure characterized by the formation of significant cracks.

Initially, these cracks initiated at the bottom surface facing upward, then propagated to the top surface, and eventually extended towards the upper rear surface before reaching the lower surface. As the applied torque increased, these cracks grew in both length and width, with most of them exhibiting an inclination of approximately 43 degrees. It is worth noting that this failure mode has been consistently documented in numerous prior studies [4,18].

In contrast, the specimens constructed with PF concrete displayed distinct behavior as the applied torque increased. Several smeared inclined cracks began to appear along the sides of the beams. Unlike the reference beams, the presence of PF played a crucial role in resisting post-cracking torque and reducing the width of the primary cracks by redirecting them into smaller, higher-density cracks. Notably, it was observed that the crack density in the beams exhibited a direct correlation with the increase in PFR content.

Furthermore, it is important to emphasize that the density of cracks in normal strength specimens exceeded that in high-strength specimens. This difference may be attributed to the increased ductility capacity of the PFR specimens. It is pertinent to mention that all tested beams ultimately failed in shear, which is a typical mode of failure for beams subjected to pure torsion.

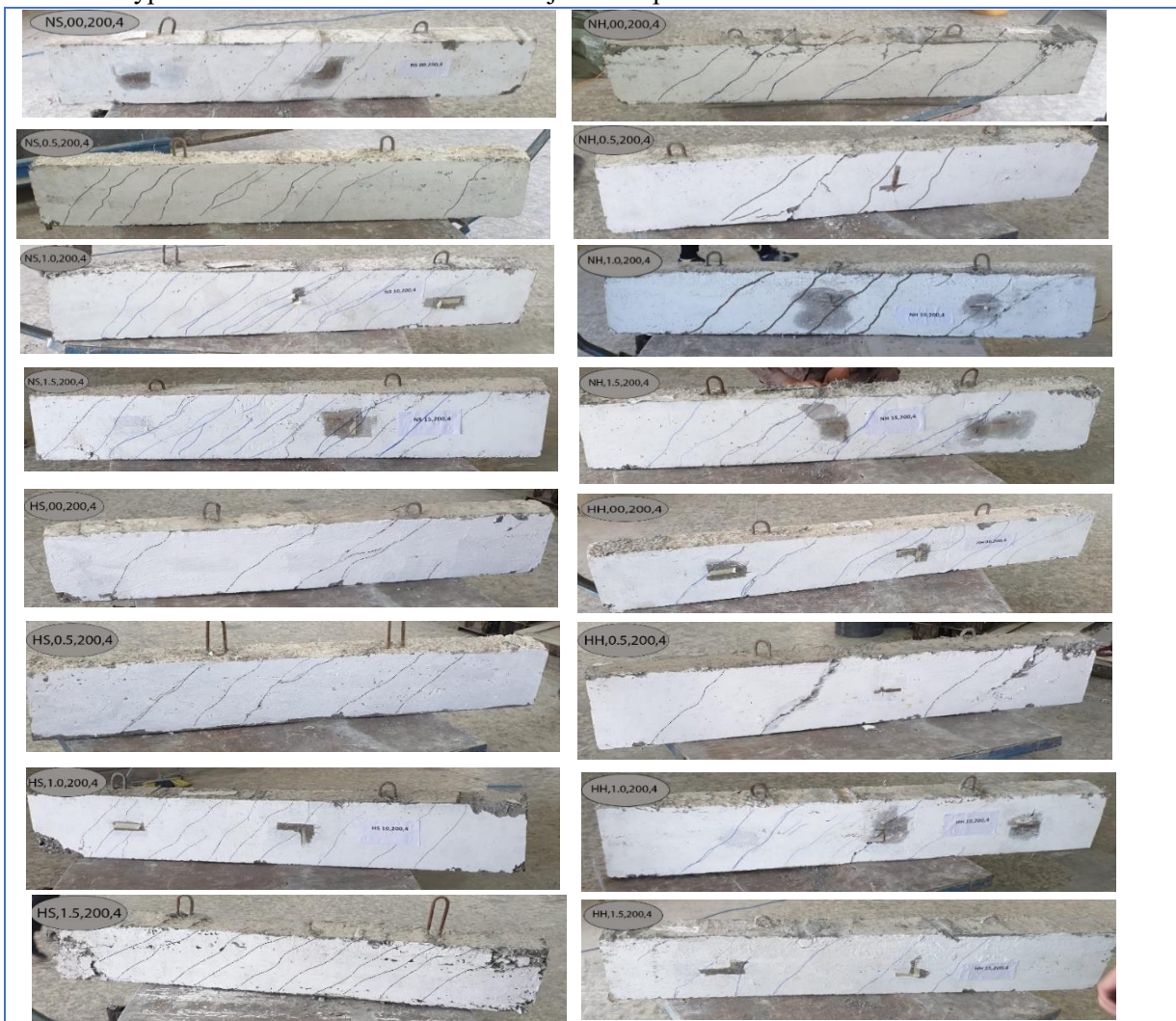


Figure 23 Failure modes of experimental testing under torsional loads

5. Conclusions

This study investigates the impact of beam type sections (hollow or solid sections) and varying fiber volume fractions on the torsional capacity of concrete specimens with normal and high strength. To sum up the key findings concisely:

The introduction of PF had a negligible effect on the concrete's compressive strength. However, it significantly enhanced the splitting tensile strength and flexural strength of PF-reinforced concrete.

1. Considerable improvements in torsional performance were observed in both solid and hollow beams, with the enhancements becoming more pronounced as the PF content gradually increased from zero to 1.5%.
2. When PFs were incorporated into high-strength concrete beams, the reduction in torsional strength between hollow and solid sections became more prominent. In contrast, in normal-strength concrete beams, the reduction ratio decreased.
3. As the fiber content increased, a relatively consistent reduction in the decrement ratio was observed in high-strength concrete. In contrast, the decrement ratio decreased in normal-strength concrete, reaching a value of 5.4% at a fiber content of 1.5%.
4. In the absence of fibers, the reduction in torsional strength was more significant in normal-strength concrete beams compared to high-strength ones. However, the presence of polyolefin fibers altered this pattern, making the reduction ratio in torsional strength more pronounced in high-strength beams compared to normal-strength beams.

References

- [1] Al-Saraj W. K. "Structural Behavior of RPC T-beams Under Pure Torsion" Ph.D. Thesis, Al-Mustansiriya University, p.189, 2013.
- [2] Allawi A., "Nonlinear Analysis of Reinforced Concrete Beams Strengthened by CFRP in Torsion", Ph.D. Thesis, University of Baghdad, p.213, 2006.
- [3] Hii K. Y. and Al-Mahaidi R., "An Experimental and Numerical Investigations on Torsional Strengthening of Solid and Box-Section RC Beams Using CFRP Laminates." *Journal of Composite Structures*, (Article in Press) , 2006.
- [4] Mazin Diwan Abdullah, Fareed Hameed Majeed and Samoel Mahdi Saleh, "The Role of Fiber-Type Reinforcement in the Torsional Behavior of Solid and Hollow Reinforced Concrete Beams." *Fibers* **2022**, 10, 80.
- [5] ASTM C150/C150M-18; Standard Specification for Portland Cement. ASTM International: West Conshohocken, PA, USA, 2018.
- [6] ASTM C150/C150M-18; Standard Specification for Concrete Aggregates. ASTM International: West Conshohocken, PA, USA, 2018.
- [7] Ding, L.; He, W.; Wang, X.; Cheng, F.; Wu, Z. Flexural behavior of reinforced concrete slabs strengthened with BFRP grids and [PCM]. *J. Cent. South Univ.* **2020**, 51, 1085–1096.
- [8] Lau, C.K.; Htut, T.N.S.; Melling, J.J.; Chegenizadeh, A.; Ng, T.S. Torsional behavior of steel fiber reinforced alkali activated concrete. *Materials* **2020**, 13, 3423. [[CrossRef](#)] [[PubMed](#)]
- [9] Lubliner, J., Oliver, J., Oller, S., Onate, E. (1989). A plastic-damage model for concrete. *International Journal of Solids and Structures*, 25(3): 299-326. [https://doi.org/10.1016/0020-7683\(89\)90050-4](https://doi.org/10.1016/0020-7683(89)90050-4).

-
- [10] Lee, J., Fenves, G.L. (1998). Plastic-damage model for cyclic loading of concrete structures. *Journal of Engineering Mechanics*, 124(8): 892-900. [https://doi.org/10.1061/\(ASCE\)0733-9399\(1998\)124:8\(892\)](https://doi.org/10.1061/(ASCE)0733-9399(1998)124:8(892))
- [11] EN 1992-1-1 (2004) (English): Eurocode 2: Design of concrete structures - Part 1-1: General rules and rules for buildings.
- [12] Hafezolghorani, M., Hejazi, F., Vaghei, R., Jaafar, M.S.B., Karimzade, K. (2017). Simplified damage plasticity model for concrete. *Structural Engineering International*, 27(1): 68-78.
- [13] Pang, X.B.D., Hsu, T.T. (1995). Behavior of reinforced concrete membrane elements in shear. *Structural Journal*, 92(6):665-679.
- [14] Belarbi, A., Hsu, T.T. (1994). Constitutive laws of concrete in tension and reinforcing bars stiffened by concrete. *Structural Journal*, 91(4): 465-474.
- [15] British Standards Institution. (2005). BS EN 1992-1-2. Eurocode 2: Design of concrete structures. Part 1-2: General rules.
- [16] Genikomsou, A.S., Polak, M.A. (2015). Finite element analysis of punching shear of concrete slabs using damaged plasticity model in ABAQUS. *Engineering Structures*, 98:38-48.
- [17] Mohsin, M.S., Alwash, N.A., Kadhum, M.M. (2021). Comparative study on structural behavior of reinforced concrete straight beam and beams with out of plane parts. *International Journal of Engineering, Transactions A: Basics*, 34(10): 2280-2293.
- [18] David Darwin, Charles W. Dolan, and Arthur H. Nilson" *Design of Concrete Structures*" Published by McGraw-Hill Education, 2 Penn Plaza, New York, NY 10121/ Fifteenth Edition (2016).